



Poly(phenylene) synthesized using diels-alder chemistry and its sulfonation: Sulfonate group complexation with metal counter-ions, physical properties, and gas transport



Timothy Largier^a, Fei Huang^b, Wayz Kahn^c, Chris J. Cornelius^{c,*}

^a Foster Corporation, Putnam, CT 06260, USA

^b Department of Chemistry and Biochemistry, University of South Carolina, Columbia, SC 29208, USA

^c Department of Chemical and Biomolecular Engineering, University of Nebraska-Lincoln, Lincoln, NE 68588, USA

ARTICLE INFO

Keywords:

Polyphenylene and sulfonated polyphenylene
Sulfonate group metal-ion complexation
Film thermal stability and physical properties
Gas transport

ABSTRACT

Sulfonated poly(phenylene) (sPP) thermal stability, physical properties, and gas transport characteristics were evaluated as a function of ion-exchange capacity ($x = \text{IEC}$), and counter-ion type ($M = \text{H}^+, \text{Cs}^+, \text{Na}^+, \text{Mg}^{2+}$, and Al^{3+}). Counter-ion substitution with its sulfonated groups produced $\Delta\nu(\text{SO}_3^-)$ vibrational shifts that were related to ion type and valence observed using FTIR. Increasing IEC and counter ion complexation strength within sPP led to greater density and reduced fractional free volume (FFV). sPPx-M exhibited a single thermal degradation step greater than 550 °C that decreased with increasing IEC. Unsulfonated poly(phenylene) (PP) had a glass transition at 391 °C, which shifted to 420 °C upon sulfonation. Thermal stability and mechanical properties increased with counter-ion type in the following order: sPP2.5-Cs⁺ < sPP2.5-Na⁺ < sPP2.5-Mg²⁺. However, decreased thermal stability and physical properties were observed using Al³⁺ as a counter-ion (sPP2.5-Al³⁺). He, H₂, CO₂, N₂, O₂ and CH₄ permeability decreased within sPP2.5-M based upon counter-ion type, size, and valence. Larger CO₂ and H₂ molecules were more permeable than He, which revealed a more complex transport process was occurring within sPP2.5. Metal-ion complexation with sPP2.5 significantly reduced CO₂ and H₂ permeability. PP possessed high CO₂ permeability (152 Barrers) with moderate CO₂/CH₄ selectivity (12.6). sPP2.5-Na⁺ (IEC = 2.5 meq/g) had a CO₂/CH₄ selectivity of 71.3, and counter-ion substitution to create sPP2.5-Cs⁺ increased CO₂/CH₄ selectivity by 23%. Gas solubility and diffusivity decreased with increasing IEC and metal-ion complexation strength. sPPx-M had tunable ideal gas permselectivity that was largely a function of sulfonate group concentration and counter-ion type.

1. Introduction

Numerous industrial processes require gas purification by selective separation between molecules [1]. Polymer membrane based gas separation processes are low cost, energy efficient, and environmentally friendly versus traditional methods [2–6]. The greatest challenge facing their development is the need for a simultaneous increase in gas permeability (P) and selectivity. This has inspired material research efforts seeking to improve the understanding of interrelationships between polymer composition, morphology, and gas permselectivity. High P may result from elevated fractional free volume (FFV), which reduces the required membrane area and energy required for gas transport. Material modification efforts are directed at controlling gas selectivity, diffusion, and solubility to fine tune its transport properties.

Ionomer composition is vital to its physical properties, which may

exhibit a diversity of new properties once complexed with a counter-ion. It's been shown that doping a sulfonated polymer with a metal-ion affects its gas selectivity and physical properties [7–12]. The vast majority of membrane research for gas separations has focused upon modifying existing polymers. There are notable efforts discussing the effect of sulfonation on gas transport phenomena that includes Nafion [7–10], poly(phenylene oxide) [13,14], and polystyrene [15]. The ionic interactions between ionomer chains increased backbone rigidity and polymer density, but may cause a decrease in its FFV. Furthermore, a large metal-ion will occupy an increasing volume between neighboring functional groups and polymer chains that will alter its transport properties. For example, Fan and Cornelius showed that Nafion-117 (N117) neutralized with Li⁺, Na⁺, K⁺, and Ca²⁺ maintained an average d -spacing. However, it led to improved thermal stability, and increased P due to losses in crystallinity [7]. N117 complexed with a

* Corresponding author.

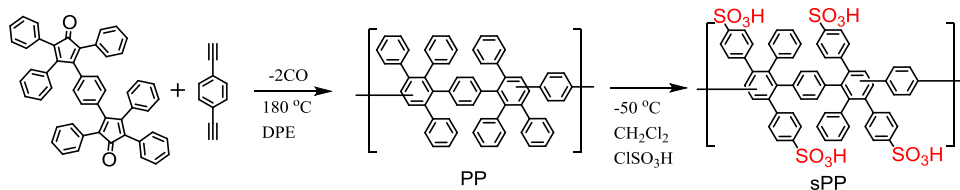
E-mail address: ccornelius2@unl.edu (C.J. Cornelius).

<https://doi.org/10.1016/j.memsci.2018.11.024>

Received 21 September 2018; Received in revised form 5 November 2018; Accepted 10 November 2018

Available online 14 November 2018

0376-7388/ © 2018 Elsevier B.V. All rights reserved.



Scheme 1. Polymerization reaction between bis(cyclopentadienone) and diethynyl benzene to form poly(phenylene) (PP). Sulfonation of PP to create a sulfonated poly(phenylene) (sPP).

divalent Ca^{2+} had a distinct impact upon chain mobility and a larger shift in the sulfonated group vibrational energy as compared to monovalent ions. Overall, Nafion gas permeability increased in the following order: $\text{N117-Li}^+ > \text{N117-Ca}^{2+} > \text{N117-Na}^+ > \text{N117-K}^+$. Similar work with Nafion neutralized with K^+ led to reduced gas diffusivity (D) and higher solubility (S) than its free acid form [10]. Rhim et al. used sulfonated poly(2,6-dimethyl-1,4-phenylene oxide) (sPPO) to examine the role of cation species upon P [14]. sPPO complexed with divalent cations had greater CO_2/CH_4 selectivity than monovalent ones. Park et al. complexed sulfonated polysulfone (sPSF) with sodium at an ion-exchange capacity (IEC) of 1.12 (meq/g) to create sPSF- Na^+ . The sPSF- Na^+ membrane had a CO_2/N_2 selectivity increase from 25.7 to 28.7 [16]. The work revealed that sPS complexed with monovalent metal ions had a greater P than multivalent ions. Hamad et al. studied gas transport properties of sulfonated poly(phenylene oxide) (sPPO) complexed with monovalent, divalent, and trivalent metal ions (H^+ , Li^+ , Cs^+ , Mg^{2+} , Ca^{2+} , Ba^{2+} , and Al^{3+}) at an IEC of 1.73. Its sulfonation increased CO_2/CH_4 ideal selectivity from 17.3 to 26.7 as well as other properties [13]. Membrane gas permselectivity variation was assumed to be caused by metal cation size and electronegativity differences altering ionic bond strength and cross-linking that caused greater hindrance to gas transport. Overall, sPPO sulfonated groups complexed with metal cations significantly affected its density and gas permselectivity. Fan and Cornelius complexed poly(*t*-butyl styrene-*b*-ethylene-*co*-propylene-*b*-styrene-*co*-styrene sulfonate-*b*-ethylene-*co*-propylene-*b*-*t*-butyl styrene) with Li^+ , Na^+ , K^+ , and Ca^{2+} [17]. Gas permeability decreased within this pentablock copolymer (PBC) if complexed with a divalent ion such as Ca^{2+} versus a monovalent ion of similar ionic radius (Na^+). For example, a smaller Li^+ ion complexed with a $-\text{SO}_3\text{H}$ group within PBC led to a lower P as compared to Na^+ and K^+ . However, a divalent Ca^{2+} ion had lower P than a Na^+ ion of similar size. Their work demonstrated that divalent ions interact quite differently than monovalent ones with sulfonated groups. One of these differences was attributed to the creation of ionic cross links that are impossible with a monovalent ion. These research efforts reveal the tunability of sulfonated polymers using ion complexation that can be used to improve gas separation properties.

Poly(phenylene)s are amorphous and rigid materials with elevated thermochemical and mechanical stability. This material has been shown to exhibit promising gas separation performance with high P and moderate selectivity [20]. Despite being under consideration for several applications [18–26], their gas transport performance has been poorly described. This study examines the effect of sulfonated poly(phenylene) (sPP) ion concentration and counter-ion size upon ion complexation strength, and bulk physical and thermal properties. sPP membrane ideal gas P , diffusivity (D), and S are evaluated using He, H_2 , O_2 , CO_2 , N_2 , and CH_4 . Ideal gas selectivity is compared with several current membrane materials.

2. Experimental

2.1. Materials

1,4-Diethynylbenzene (Fischer Scientific, 95%) was purified by sublimation prior to use. 1,3-Diphenylacetone (99%), acetone ($\geq 99.5\%$), toluene ($\geq 99.5\%$), tetrahydrofuran (99.9%) and methanol ($\geq 99.8\%$)

were purchased from Fisher Scientific and used as received. Diphenyl ether, chlorosulfonic acid, dimethylacetamide (DMAc), and anhydrous methylene chloride were used as received from Aldrich. Dichloromethane (99.9%) and diphenyl ether (99%) were purchased from Acros Organics and used as received. Bis(cyclopentadienone) monomers were synthesized according to previously published literature by corresponding author [24–26].

2.2. Poly(phenylene) synthesis, molecular weight, and composition

An example poly(phenylene) (PP) synthesis was performed using an equimolar mixture of bis-tetracyclone (50.0 g; 72.4 mmol) and 1,4-diethynylbenzene (9.13 g; 72.4 mmol). These monomers were added to a 500 mL three-neck containing 250 mL of diphenyl ether (DPE). A Diels-Alder reaction was performed with these monomers under an Argon atmosphere at 180 °C with continuous stirring. The solution's color changed from dark purple-brown to orange after four hours. However, the reaction was allowed to continue for an additional 24 h to maximize its conversion and molecular weight. Overall stoichiometry and predicted molecular weight was controlled using Carother's equation. After the reaction was completed the polymer solution was cooled to room temperature (RT) and diluted using toluene. The dilute solution was filtered by centrifuging at 9000 rpm for 30 min to remove unreacted solids. The clear polymer-solvent solution was precipitated in acetone to give poly(phenylene) (PP) shown in Scheme 1. The white solid was dried in a vacuum oven for 48 h at 200 °C and stored at RT. Additional PP synthesis details are reported elsewhere [24–28].

PP molecular weight and distribution were obtained using an Agilent 1260 GPC/SEC System fitted with a TL105 HPLC column heater from Timeberline Instruments®. The system consisted of a series of two linear PSS® SDV columns, with a porosity of 1000 Å and 100,000 Å. The column combination has a separation range of 100–1000,000 Da. A twelve point calibration curve, obtained within one day of data collection, was obtained using poly(styrene) standards with a molecular weight range of 474–2520,000 Da from PSS® (PSS-pskitr1). The GPC was run with a tetrahydrofuran (THF) mobile phase at a column temperature of 25 °C. The flow rate was 1 mL/min using an injection volume of 100 µL. PP was dissolved in THF to create a 0.1 wt% solution that was filtered using a 0.45 µm PTFE filter prior to its injection into the column. GPC results gave a PP weight average molecular weight (M_w) of 192,000 g/mol with a polydispersity index (PDI) of 2.4. Its number-average molecular weight (M_n) was 78,000 g/mol.

PP composition and polymerization characteristics were analyzed using ^1H NMR with a Bruker Avance III-HD 400 MHz NMR in CD_2Cl_2 . Its ^1H NMR spectra had broad aromatic protons from $\delta = 7.5$ –6.1 ppm shown in Fig. 1. The polymer's regiochemistry was due to 1,4-diethynylbenzene that produces isomers observed in other studies [28]. The PP peak assignments and ^1H NMR ($d\text{-CD}_2\text{CL}_2$) δ (ppm) is a broad signal ranging from 6.35 to 7.22 (peaks at 7.42, 7.18, 7.11, 7.06, 6.96, 6.89, 6.82, 6.68, 6.62, 6.35, 6.28, 6.20).

2.3. Poly(phenylene) sulfonation

The PP repeat unit has six pendent phenyl groups that have the possibility of being sulfonated (Scheme 1). Its sulfonation is believed to be at the para-positions of the pendant phenyl groups due to steric

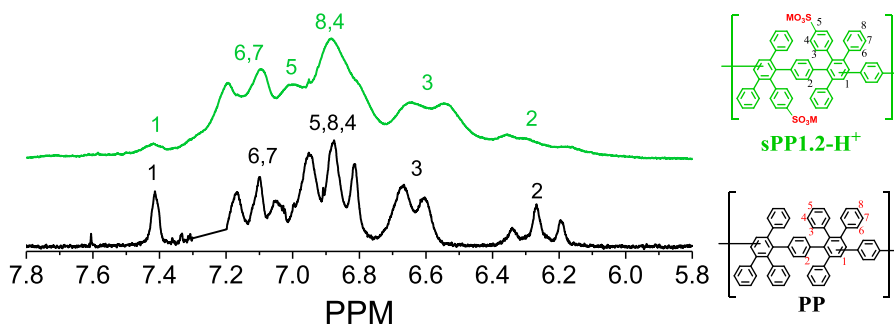


Fig. 1. ^1H NMR spectra of PP and sPP1.2- H^+ .

interference created by the rigid rod backbone (Scheme 1). This theoretically limits its sulfonation between 0 and 6 sulfonic acid groups per repeat unit with a maximum IEC of 4.954. Its degree of sulfonation is controlled by the molar ratio of ClSO_3H to PP repeat unit. PP sulfonation has been previously reported using chlorosulfonic (ClSO_3H) in chloroform [26]. Stoichiometric ClSO_3H amounts were used to create ionomers with an IEC of 1.22, 1.76, and 2.49 (meq/g). Sulfonated PP (sPP) is designated as sPPx where x represents its theoretical IEC. The general sulfonation approach involves creating a 5 wt% PP solution in CH_2Cl_2 . An example synthesis of sPP involved dissolving 9.00 g (11.8 mmol) of PP into 135 mL of CH_2Cl_2 in a flame dried 3-neck round bottom that is equipped with a mechanical stirrer. The reaction solution was continuously purged with argon, and its temperature set to approximately -79°C . A ClSO_3H (4.13 g, 35.48 mmol) and CHCl_3 (5 mL) solution was slowly added drop-wise into the PP solution. The reaction mixture was continuously stirred and allowed to slowly come to RT. The organic phase was decanted from a solid precipitate. A 0.5 M NaOH solution (300 mL) was added to the reaction vessel and stirred for 24 h in order to completely neutralize sPP and excess acid. This process converts sPPx from its acid form to Na^+ form (sPPx- H^+ into sPPx- Na^+) by neutralizing its sulfonate group ($\text{R-SO}_3\text{H}$ to $\text{R-SO}_3\text{Na}$). The tan precipitate was collected and washed with deionized (DI) water several times until the solution was neutral; and all residual salt and NaOH were removed from sPPx. The %Sulfonation was calculated from the measured experimental IEC, molecular weight of the repeat unit (MW_{RU}), and maximum theoretical IEC of sPPx if all six pendant groups were sulfonated (IEC = 4.954). The sPPx series created in this work are summarized in Table 1.

sPP1.2- H^+ was analyzed in deuterated dimethylsulfoxide (DMSO-d_6) using ^1H NMR shown in Fig. 1. Comparing the ^1H NMR spectra for PP and sPP1.2- H^+ , no significant changes in peak positions was observed. However, overall peak broadening was observed after PP sulfonation. This is due to a change in PP polarity after functionalization with sulfonic acid (SO_3H) groups, and NMR solvent change from CDCl_3 for PP to DMSO-d_6 for sPP due to solubility issues. The ^1H NMR signals for sPP ranged from 6.35 to 7.42 ppm. The five (5-C) signal position associated with PP shifted within sPP due to 5-H protons being replaced by sulfonic acid groups. Attempts were made to identify the specific sulfonic acid group attachment within PP using 2-dimensional (2D) ^1H NMR. However, the 2D ^1H NMR spectrum revealed very little information about SO_3^- group regioselectivity due to signal broadening and overlapping peaks.

Table 1
sPPx sample IEC and % sulfonation.

Sample	IEC (meq/g)	MW_{RU} (g/mol)	% Sulfonation
sPP1.2	1.22	872	24.6
sPP1.8	1.76	921	35.5
sPP2.5	2.49	987	50.3

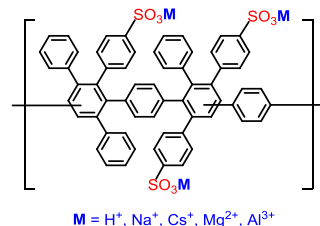
2.4. Film formation

The sPPx- Na^+ was dissolved in DMAc (10 wt%) and filtered using a 5 μm PTFE syringe filter. The particle-free polymer solution was evenly spread within a clean glass plate and its thickness was controlled using solution concentration and casting area. Films were formed using a vacuum oven at 50°C for 24 h with continuous solvent removal. Solid sPPx- Na^+ films were heated in a vacuum at 200°C for 12 h to ensure complete removal of residual solvent and water. The nominal sPPx film thickness was 3.0 mil (76.2 μm) used for all experiments.

The following procedure was used to exchange the counter-ion of sPP2.5- Na^+ , sPP1.8- Na^+ , and sPP1.2- Na^+ with another counter-ion ($\text{M} = \text{H}^+, \text{Na}^+, \text{Cs}^+, \text{Mg}^{2+}, \text{and Al}^{3+}$). The first step involves converting a sPPx- Na^+ film into sPPx- H^+ by soaking it within a 1 M H_2SO_4 solution at 90°C for 2 h. After this solid-state conversion step, all sPPx- H^+ films were treated in boiling deionized (DI) H_2O , and rinsed multiple times at RT in DI H_2O to remove all residual acid before exchanging its H^+ ion with a metal ion. sPPx- H^+ films had their H^+ exchanged by solid-state conversion using NaCl, CsOH, MgCl_2 , and $\text{Al}(\text{OH})_3 \cdot x(\text{H}_2\text{O})$ to produce sPPx- Na^+ , sPPx- Cs^+ , sPPx- Mg^{2+} , and sPPx- Al^{3+} . The sPPx- H^+ conversion process involved heating a film in either 1 M NaCl (sodium chloride crystalline/certified ACS, Fisher Sci.), 1 M CsOH (cesium hydroxide monohydrate 99.5%, ACROS Organics), 1 M MgCl_2 (magnesium chloride hexahydrate $^+99\%$ crystalline/certified ACS, ACROS Organics), or 1 M $\text{Al}(\text{OH})_3 \cdot x(\text{H}_2\text{O})$ (50–57.5% aluminum hydroxide hydrate Sigma-Aldrich) solution at 60°C for 1 h. Excess metal-ion was removed from all treated films by boiling in DI H_2O for 2 h, which was followed by soaking in DI H_2O for 24 h. The final sPPx-M film was initially dried at ambient conditions that was followed by drying at 200°C for 24 h under vacuum. The van der Waal's radius ($\text{vdw}_{\text{radius}}$) and molar mass of Na, Cs, Mg, and Al are 22.99 g/mol ($\text{vdw}_{\text{radius}} = 120 \text{ pm}$), 312.91 g/mol ($\text{vdw}_{\text{radius}} = 343 \text{ pm}$), 24.31 g/mol ($\text{vdw}_{\text{radius}} = 173 \text{ pm}$), and 26.98 g/mol ($\text{vdw}_{\text{radius}} = 184 \text{ pm}$). The final sPPx-M material is shown in Scheme 2.

2.5. Material characterization

Fourier-transform infrared spectroscopy (FT-IR) was performed to characterize metal-ion complexation with sulfonated groups within sPP. A Nexus 670 ThermoNicolet FTIR with a deuterated triglycine



Scheme 2. Idealized structure of sPPx-M.

sulfate (DTGS) detector and KBr beamsplitter was used to collect spectra. The equipment was operated an aperture diameter of 8 mm with an approximate area of 0.50 cm². For each sample, 50 scans were performed over a spectral range of 4000–400 cm⁻¹.

Film thermal stability was assessed using a TA Instruments model Q 500 Thermo Gravimetric Analyzer (TGA). Sample mass for testing ranged between 10 and 15 mg. All samples were initially held at 200 °C for 30 min using a N₂ atmosphere flowing at 20 mL/min. After material equilibration, all samples were thermally ramped at 10 °C per minute to 800 °C.

A TA Instruments Dynamic Mechanical Analyzer (DMA) Q800 was used to assess film physical properties. A thermal DMA analysis was performed in tensile mode at a frequency of 1 Hz using a N₂ atmosphere. Prior to a test, all samples were equilibrated at 115 °C for 30 min before ramping temperature at 1 °C per minute to 450 °C. The test film length and width was approximately 10 mm and 2.5 mm with a thickness of 75 μm.

The IEC of sPPx-H⁺ was measured by titrating it using a known volume and concentration of NaOH (C_{NaOH}). This solution became acidic as R-SO₃H groups were converted into R-SO₃Na H⁺ as H⁺ ions diffused into the media over a 24 h period. The acidic solution was titrated with an appropriate volume of 0.01 M NaOH (V_{NaOH}) needed to neutralize it to a pH = 7.0. The initial sPPx-H⁺ dry mass (W_d) was recorded prior to neutralizing it. The experimentally determined IEC is given by Eq. (1) and data summarized in Table 1.

$$IEC \text{ (meq/g)} = \frac{V_{NaOH} C_{NaOH}}{W_d} \quad (1)$$

PP and sPPx density (ρ) measurements were collected using a Mettler Toledo XS205 analytical balance fitted with a Mettler density kit. The measurement is based upon Archimedes' principle that relates a sample's dry mass (m_{A1}) measured in air with its buoyant mass (m_{A2}) evaluated within an auxiliary liquid. These changes are related to the densities of the auxiliary liquid (ρ_{aux}), air density (ρ_{air} = 0.0012 g/cm³), and ρ. The ρ relationship between air, liquid, and sample mass is given by Eq. (2). Prior to a density measurement, all materials were dried in a vacuum oven at least one day at 200 °C. Heptane was used as the auxiliary liquid because no film was soluble in it. The solution and film were allowed to come to equilibrium at 25 °C before measuring the buoyant mass. The experimental error was approximately 0.008 g/cm³ (1.2%), which was attributed to surface wetting characteristics. The specific volume (V) is the inverse of the polymer density (V = 1/ρ). The polymer mass was adjusted by the amount of moisture within the materials determined by TGA. These results are summarized in Table 2.

$$\rho = \frac{m_{A1}}{m_{A1} - m_{A2}} (\rho_{aux} - \rho_{air}) + \rho_{aux} \quad (2)$$

Ionomer and polymer FFV were estimated using Eq. (4) based upon its measured V, estimated occupied volume (V_o) using group contribution theory (GCT), and molecular weight of its repeat unit (M_{ru}) [17]. V_o is the van der Waals volume (V_w) for each structural group's contribution (k) and their total number (K) that are summarized in

Table 2
PP and sPPx-M calculated ρ, V, ρ*IEC, V_o, and FFV.

	ρ (g/cm ³)	V (cm ³ /g)	ρ*IEC (mmol/cm ³)	V _o (cm ³ /g)	FFV
PP	1.105	0.905	0.00	0.602	0.335
sPP1.2-H ⁺	1.247	0.802	1.50	0.582	0.274
sPP1.8-H ⁺	1.308	0.765	2.35	0.575	0.248
sPP2.5-H ⁺	1.413	0.708	3.52	0.567	0.199
sPP1.2-Na ⁺	1.319	0.758	3.28	0.567	0.252
sPP1.8-Na ⁺	1.460	0.685	3.64	0.567	0.172
sPP2.5-Na ⁺	1.519	0.658	3.78	0.567	0.139
sPP2.5-Cs ⁺	1.640	0.610	4.08	0.567	0.070
sPP2.5-Mg ²⁺	1.690	0.592	4.21	0.567	0.042
sPP2.5-Al ³⁺	1.322	0.756	3.29	0.567	0.251

Table 3
V_w and M_{ru} for various structural groups.

Structural group	V _w (cm ³ /mol)	M _{ru} (g/mol)
Phenyl	45.9	45.9
Phenyl (para/meta)	43.3	43.3
Phenyl (trisub.)	40.8	40.8
Phenyl (pentasub.)	- 4.6	- 4.6
-SO ₃ H	28.3	28.3

Table 3. A constant 1.3 is an estimate to account for molecular crystal packing density being greater than its molecular volume at absolute zero. The predicted material's FFV and V_o are summarized in Table 2.

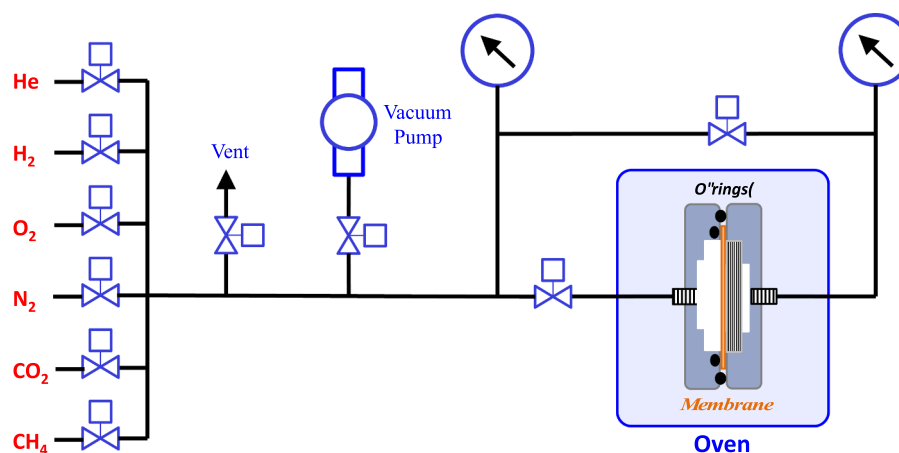
$$FFV = 1 - (V_o/V) = 1 - \left[1.3 \sum_{k=1}^K (V_w)_k / M_{ru} \right] \rho \quad (4)$$

Gas transport properties were obtained using a custom built gas permeation system shown in Scheme 3. The system utilized the time-lag technique, which was used to measure gas P, D, and S based upon the time-lag technique [29–31]. Gases used in this study were He, H₂, O₂, CO₂, N₂, and CH₄ with a purity of 99.999% (ultra-pure, Matheson Tri-Gas®). All film samples were heated to 200 °C under vacuum for 24 h prior to testing to remove all residual water. All test films were immediately mounted in a cell to ensure that no water was absorbed in any tested film. Feed pressure was preset to an absolute pressure of 4 atm and a constant temperature of 30 °C. The automated gas permeation test was controlled and programmed utilizing LabVIEW graphical interface programming software. The reproducibility in measuring P was found to be approximately 5%. Greater details regarding this system and its operation have been published elsewhere [29,30].

3. Results and discussion

3.1. FTIR of PP and sPPx-M

Ionomer compositional changes due to PP sulfonation into sPPx-H⁺ were evaluated using FTIR shown in Fig. 2 and summarized in Table 2. A phenyl group's carbon-carbon (CC) stretching typically occurs around 1500–1400 cm⁻¹. The IR spectrum confirms the presence of sulfonate groups that have increasing intensity with IEC due to absorption within sPPx. There is little change in the stable aromatic carbon-carbon bonds (ν(CC)) located from 1400 to 1600 cm⁻¹. The IR spectra of PP and sPPx have a carbon-hydrogen (CH) out-of-plane vibration near 767 cm⁻¹ that corresponded to the five adjacent aromatic hydrogen-carbon (ν(CH)) bonds of the pendant phenyl groups [26,29,32]. A 1,4-phenyl peak (1,4-ph) is attributed to the backbone of PP and sPPx observed at 842 cm⁻¹ that does not change with sulfonation level. The phenyl out-of-plane C-H peak at 899 cm⁻¹ diminished in sPPx as hydrogen groups are lost due to sulfonation. This peak intensity decrease with IEC suggests that sulfonation is occurring predominately on the pendent phenyl groups due to the conversion of mono-substituted phenyl rings into di-substituted ones. sPPx has a S-O stretch at 1002 cm⁻¹ and 1033 cm⁻¹ due to the sulfonate group being attached to a pendant PP phenyl group. The asymmetric and symmetric sulfonate group stretching is noted at 1125 cm⁻¹ and 1105 cm⁻¹ that increased with sPPx sulfonation. The S'O sulfonate group's asymmetric and symmetric stretching (ν(SO₃)) was observed at 1125 cm⁻¹ and 1174 cm⁻¹. PP and sPPx had carbon-carbon stretching of their phenyl group at 1443 cm⁻¹ and 1433 cm⁻¹, which has been shown to occur between 1500 cm⁻¹ to 1400 cm⁻¹ for other phenylated materials [26]. This vibration corresponds to the sPPx and PP backbone that had little change in its stable aromatic C=C bonds. The unchanging 1443 cm⁻¹ and 842 cm⁻¹ peaks were used as a reference to normalize sPPx films in order to evaluate compositional differences. Overall, the IR spectra revealed that PP



Scheme 3. Schematic representation of gas permeation set-up and cell.

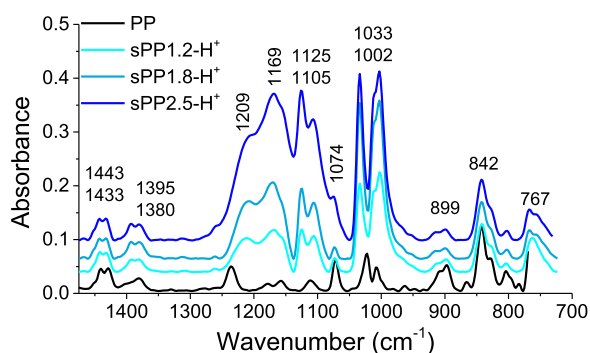


Fig. 2. FTIR spectra of PP and sPPx-H⁺ as a function of IEC.

Table 4

Primary IR band assignments of sPPx-H⁺.

ν (cm ⁻¹)	Peak assignment
767, 899	CH out of plane pendant phenyl group
842	1,4-phenyl group
1002	Symmetric stretch of SO ₂
1033	Asymmetric S-O stretch of sulfonic acid group
1074	CCH bending vibration
1105, 1125	Asymmetric and Symmetric SO ₂ stretch
1169	Symmetric SO ₃ stretching vibration [26,32,33]
1209	Asymmetric stretch of sulfonic acid group
1380, 1395, 1433, 1443	Phenyl group in-plane CC stretching

underwent conversion into sPPx at various degrees of sulfonation Table 4.

sPPx-H⁺ bond stretching and bending vibrations characterized using IR were shown to be a good technique to confirm the presence of functional groups such as -SO₃H at multiple wavenumbers. As previously noted, increasing IEC within sPPx-H⁺ produced greater sulfonated group absorption intensities with concentration (Fig. 2). The relationship between these identified peaks versus wavenumber and IEC were examined using sPPx-Na⁺ shown in Fig. 3A. The sulfonic acid group absorption changed proportionally with IEC, and small wavenumber shifts associated with the -SO₃H group. The majority of the identified peaks associated with ν (CH), ν (1,4-ph), and ν (CC) did not change significantly with regard to shape or absorption intensity. However, ν (SO₃), ν (SO₂), and ν (SO) had several notable changes related to wavenumber shifts to a higher number; and absorption intensity changes in ν (SO₂) and ν (SO) relative to ν (SO₃). In particular, ν (SO₂) became more defined as compared to sPPx-H⁺. However, the sulfonic acid group and polymer backbone IR fingerprint did not change based upon IEC and Na⁺ counter-ion. These results suggest that no residual or

free counter-ion remains within a given film, and FTIR changes are primarily due to the complexation between -SO₃-M within sPPx. In order to test this concept, Beer-Lambert Law was used to relate changes in sPPx-Na⁺ sulfonate group concentration ($c_{\text{SO}_3\text{Na}}$), film thickness (l), and observed IR absorption (A) intensity. A molar absorptivity coefficient (ϵ) is used to relate A to $c_{\text{SO}_3\text{Na}}$ and l using the expression $A = \epsilon l c_{\text{SO}_3\text{Na}}$. The ν (SO) at 1033 cm⁻¹ was chosen to be followed within sPPx-Na⁺ due to no overlapping peaks observed near this wavenumber. A plot of a film's observed A versus the product of $l \cdot [\text{IEC} \cdot \rho]$ that is equivalent to $\epsilon l c_{\text{SO}_3\text{Na}}$ is shown in Fig. 3B. An ϵ coefficient of 0.601 m²/mol found for sPPx-Na⁺, and the linear fit provides further confirmation of the successful sulfonation of PP.

The sulfonate groups vibrational mode is influenced by its local chemical environment, and counter-ion interactions that will polarize the S-O dipole [34]. This will depend upon the metal-ion radius, charge density, and valence [32–34]. Interestingly, the ν (CH), ν (CC), and ν (1,4-ph) wavenumber and absorption intensity of the aromatic group's absorption did not appear to change with counter-ion type ($M = \text{Na}^+$, Cs^+ , Mg^{2+} , and Al^{3+}) shown in Fig. 4A. This appears to indirectly indicate that complexation with -SO₃M is the dominate factor impacting its absorption characteristics. While little changes were noted at these wavenumbers, appreciable changes were observed at ν (SO₃), ν (SO₂), and ν (S-O) shown in Fig. 4A. The sulfonated group absorption intensity and wavenumber shifts associated with ν (SO₂), ν (S-O), and ν (SO₃) changed based upon the counter-ion type summarized in Table 3. In general, metal-ion complexation with sPP2.5 produces an increase in wavenumber, but sPP2.5-Al³⁺ was an exception. This deviation may be due to its higher coordination number, but Al³⁺ causes a greater decrease in the sulfonate group absorption intensity noted by ν (SO₂), ν (S-O), and ν (SO₃).

Vibration and rotational energy changes are observed as wavenumber differences for ν (SO₂), ν (SO), and ν (SO₃) based sPP2.5-M and its complexation with a metal-ion versus non-complexed that is defined as $\Delta\nu$. The changes in ν (SO₂), ν (S-O), and ν (SO₃) between sPP2.5-M and sPPx-H⁺ varied in magnitude. In order to appreciate these differences, the wavenumber shifts between ν (SO₂), ν (S-O), and ν (SO₃) for the acid form of sPP2.5-H⁺ and its salt form ($\Delta\nu$) was quantified by ideally modeling its molecular interaction energy $\Delta E = N_A h c \Delta\nu$ where N_A is Avogadro's number, h is Planck's constant, and c is the speed of light [32]. The relationship between ΔE (SO₃), ΔE (SO₂), and ΔE (S-O) versus counter-ion type and ionization energy (E_{ion}) is shown in Fig. 4B. A correlation between ΔE (SO₂) and ΔE (S-O) versus E_{ion} , electronegativity of metal-ion (X_{ion}), or its ionic size (r_{ion}) was not found to be strongly related to ΔE . Their predicted energies ranged between 12.0 J/mol (sPP2.5-Al³⁺) to 35.9 J/mol (sPP2.5-Na⁺), which did not appear to be dependent upon E_{ion} , X_{ion} , or r_{ion} . However a change in ΔE (SO₃) for sPP2.5-M ranged between 83.7 J/mol (sPP2.5-Cs⁺) to -71.8 J/mol

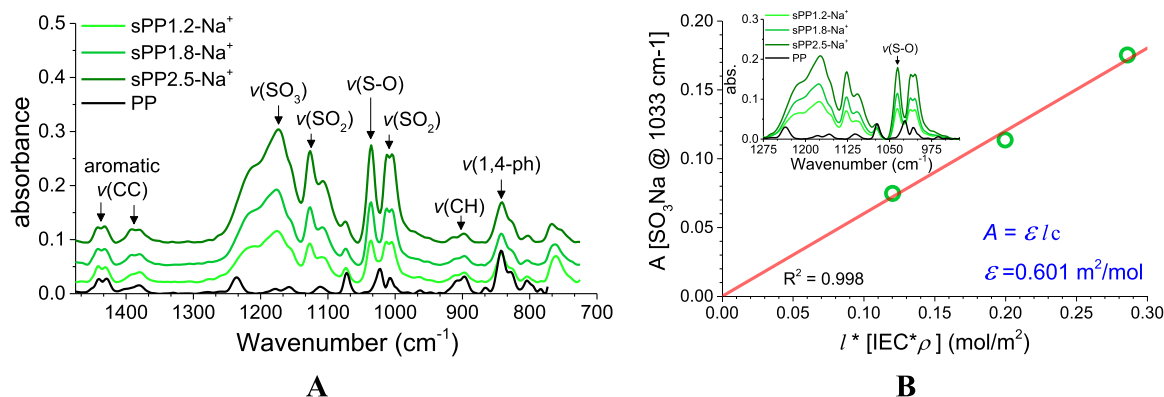


Fig. 3. A) FTIR of sPPx-Na⁺ as a function of IEC. B) Absorption intensity of sPPx-Na⁺ at 1033 cm⁻¹ versus I* [IEC*ρ].

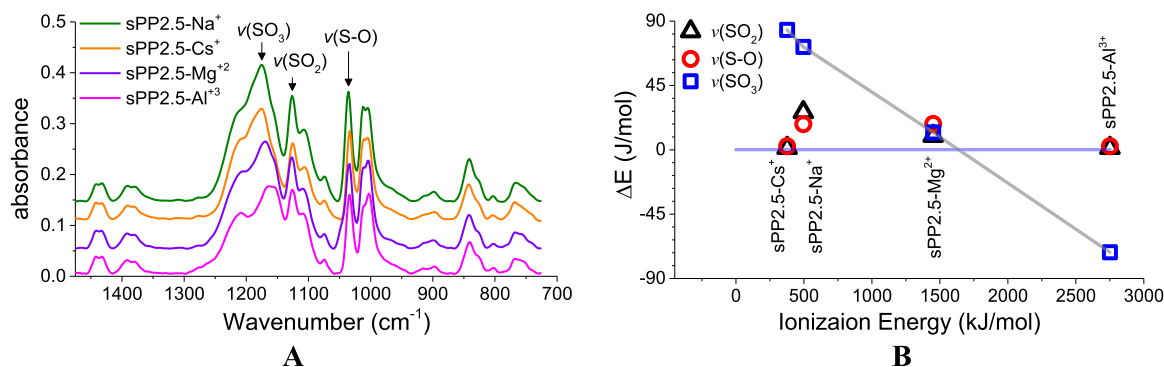


Fig. 4. A) FTIR spectra of sPP2.5-M based upon counter-ion type (M = Na⁺, Cs⁺, Mg²⁺, and Al³⁺). B) Predicted ΔE of sPP2.5-M⁺ for ν(SO₂), ν(S-O), and ν(SO₃) versus Ionization Energy.

(sPP2.5-Al³⁺), which appeared to be linearly related to E_{ion} ; and scaled with X_{ion} and r_{ion} . This correlation may be due to ν(SO₃) vibration and rotational energy modes being more sensitive to its complexation with a metal-ion. sPP2.5-M complexed with Na⁺ and Cs⁺ caused the largest change in ΔE(SO₃) from 71.3 J/mol ($E_{ion} = 376$ kJ/mol) to 83.7 J/mol (496 kJ/mol). The sPP2.5-Mg²⁺ energy changes were quite small in comparison to all materials (ΔE(SO₃) = 12.0 J/mol and $E_{ion} = 1450$ kJ/mol). Finally, sPP2.5-Al³⁺ was highly unusual because its ΔE(SO₃) was -71.8 J/mol at $E_{ion} = 2750$ kJ/mol. While a linear trend was noted

using ν(SO₃) as a reference, its relationship to hydrogen bonding and electrostatic forces is not clear and requires additional studies.

3.2. Thermal properties of PP and sPPx-M

Thermogravimetric analysis was performed to assess PP and sPPx-H⁺ thermal stability shown in Fig. 5A. PP displayed excellent thermal stability with a single degradation step at an onset temperature (T_{onset}) of 581 °C occurring at a mass loss of 5 wt%. sPPx-H⁺ had a three-stage

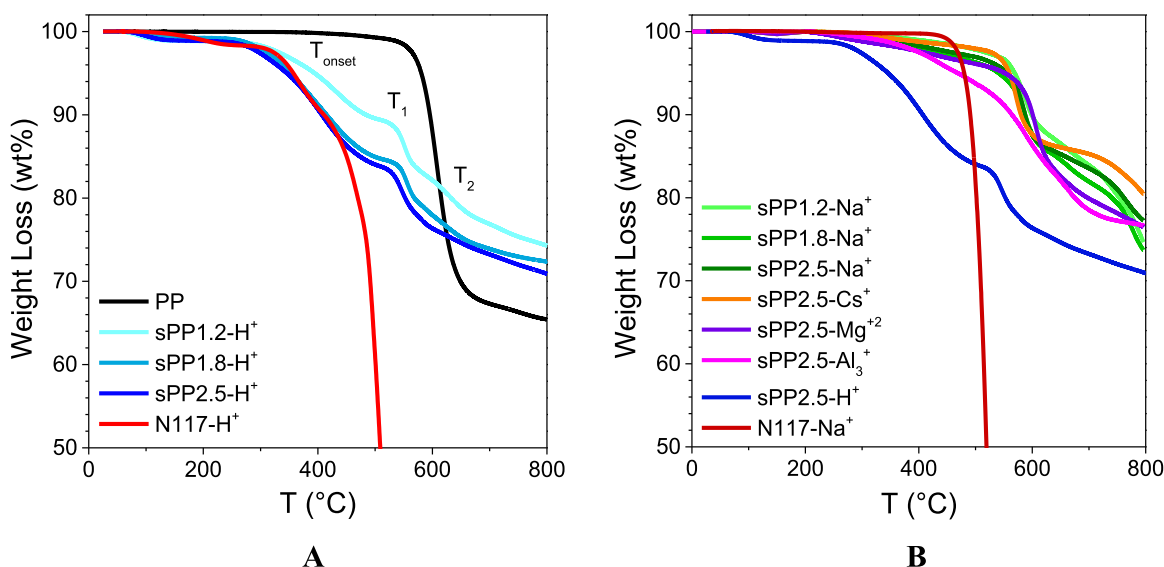


Fig. 5. TGA analysis in N₂ of A) N117-H⁺, PP, sPP1.2-H⁺, sPP1.8-H⁺, and sPP2.5-H⁺; and B) N117-Na⁺, sPP1.2-Na⁺, sPP1.8-Na⁺, sPP2.5-Na⁺, sPP2.5-Cs⁺, sPP2.5-Mg²⁺, and sPP2.5-Al³⁺.

mass loss attributed to water bonded to in the form $-\text{SO}_3\text{H} \cdot n(\text{H}_2\text{O})$ being thermally removed that is followed by decomposition. The residual water began leaving each sPPx- H^+ film at approximately 120 °C that corresponds to 3.27 kJ/mol, which is lower than N117- H^+ (4.22 kJ/mol). T_{onset} began at 393 °C for sPP1.2- H^+ that decreased to approximately 350 °C for N117- H^+ , sPP1.8- H^+ , and sPP2.5- H^+ . This behavior was attributed to the higher concentration of sulfonate groups within these materials as compared to sPP1.2- H^+ . The second thermally induced weight loss (T_1) within sPPx- H^+ is attributed to decomposition of sulfonic acid groups. This typically occurs from 285 to 426 °C in highly phenylated arylene-sulfonic polymers. The experimental T_1 for sPP1.2- H^+ , sPP1.8- H^+ , and sPP2.5- H^+ at 529 °C (88.9 wt%), 538 °C (84.7 wt%), and 525 °C (83.3 wt%) that is consistent with this literature result. Under these test conditions N117- H^+ nominally had a T_1 inflection at 437 °C at a residual mass of 87.4 wt%. The final thermal event (T_2) event appears as a change in slope at 656 °C (78.3 wt%), 657 °C (75.0 wt%), and 650 °C (74.6 wt%) for sPP1.2- H^+ , sPP1.8- H^+ , and sPP2.5- H^+ ; but, N117- H^+ lacked this thermal event. This transition was associated with sPPx- H^+ backbone degradation into carbonaceous material. The sPPx- H^+ trend shows that increased sulfonation will enhance its thermal decomposition, which has been noted for other sulfonated materials. The thermal stability of these hydrocarbon ionomers is a good physical property trait.

sPPx- Na^+ and N117- Na^+ metal-ion complexed ionomers exhibited large improvements in thermal stability (Fig. 5B). sPPx- Na^+ had a very gradual weight loss from 300 °C until a sharp degradation step at roughly 560 °C. This loss is believed to be residual water associated with the $-\text{SO}_3\text{M} \cdot \text{H}_2\text{O}$ complex. This was determined to be approximately two water molecules per sulfonate group for all sPPx- Na^+ materials. N117- Na^+ did not have this water loss that may be due to its higher chain mobility created by a lower glass transition temperature. These experiments revealed that a metal counter-ion has a pronounced effect upon sPP2.5-M thermal stability. Its observed T_{onset} was inversely proportional to counter-ion size ($\text{Mg}^{2+} > \text{Na}^+ > \text{Cs}^+$) that is consistent with literature [7,11]. This result suggests a sulfonate and metal-ion complex may impede backbone decomposition within an ionomer [35,36]. The temperature at 3 wt% loss ranged between 439 °C and 539 °C that was related to counter-ion size in the following order: $\text{Cs}^+ > \text{Na}^+ > \text{Mg}^{2+} > \text{Al}^{3+}$. This variation is believed to be due to small $-\text{SO}_3\text{M} \cdot \text{H}_2\text{O}$ complex variations related to metal-ion type because all sPP1.5-M material's thermal behavior converges to an average temperature of 567 °C at 94 wt%. This is approximately 1.5 water molecules per sulfonate group. sPP2.5- Al^{3+} differed from these materials by experiencing a more severe mass loss at a lower temperature. This

accelerated ionomer degradation was noted with N117-M complexed with multi-valent metal ions such as Al^{3+} , Sn^{4+} , and Fe^{3+} by Bas et al. Their work described stability differences in terms of an ion's Lewis acid strength (LAS), and overall stability being proportional to counter-ion size [37]. In addition to LAS affects, Al^{3+} and "other" multi-valent ions possess a charge that may not be readily neutralized in a complex such as $n[\text{RSO}_3]^- [\text{Al}]^{3+}$. This could be partially attributed to charge availability and steric hindrances. The diverse change in thermal stability with counter-ion type indicates a significantly different degradation mechanism involving weight loss (emission) and char (crosslinking). It is clear that multivalent ions lead to greater temperature sensitivity than monovalent and divalent species.

3.3. PP and sPPx-M film physical properties

PP and sPPx-M film stress-strain (σ - ϵ) curves were performed at ambient conditions in an air atmosphere shown Fig. 6A. PP had the best σ - ϵ behavior of the series that was followed by sPPx- Na^+ . These films had a high Young's moduli (E_Y) and yield stress that decreased with increasing IEC shown in Fig. 6B versus their molar volume. A reduced film E_Y is attributed to excessive water content (WC) that plasticized films and reduced their mechanical properties (Table 6). It was initially assumed that little water would be absorbed in these salt-neutralized materials at ambient conditions (25 °C) and moderate relative humidity (35% RH). This assumption was made because at these identical conditions (T and RH) sPP1.2- H^+ to sPP2.5- H^+ films had less than 1.5 wt% residual water within a film based upon TGA tests. However, there was strong relationship between sPPx-M moisture content, IEC; and counter-ion concentration and type. For example, a sPP2.5- Mg^{2+} film absorbed 24.9 wt% H_2O that was not readily removed using a vacuum oven without heat. The absorbed H_2O within these materials was attributed to hydrogen bonding, complexation with $-\text{SO}_3\text{M}$ groups, and "trapped" water. The plasticizing nature of water partially explains the decreased mechanical properties of sPP2.5-M, and the plasticity (elongation to break) observed with sPP2.5- Mg^{2+} (Fig. 6A). sPPx- Na^+ film elongation at break (ϵ_b) and E_Y decreased with IEC in the following manner: sPP2.5- Na^+ ($\epsilon_b = 0.572$ and $E_Y = 1.50$ GPa) > sPP1.8- Na^+ ($\epsilon_b = 0.471$ and $E_Y = 1.77$ GPa) > sPP1.2- Na^+ ($\epsilon_b = 0.465$ and $E_Y = 1.83$ GPa), which corresponded to 9.5 wt%, 11.8 wt%, and 16.3 wt% H_2O within each film (Table 6). sPP2.5- Mg^{2+} and sPP2.5- Al^{3+} had similar σ - ϵ curves up to $\epsilon = 25.7\%$ where sPP2.5- Al^{3+} failed at $E_Y = 1.28$ GPa. Furthermore, the sPP2.5- Al^{3+} film did not seem to follow the trend of E_Y versus V shown for other sPPx-M films shown in Fig. 6B. The sPP2.5- Mg^{2+} film had a ϵ and E_Y of 47.4% and 1.03 GPa, but

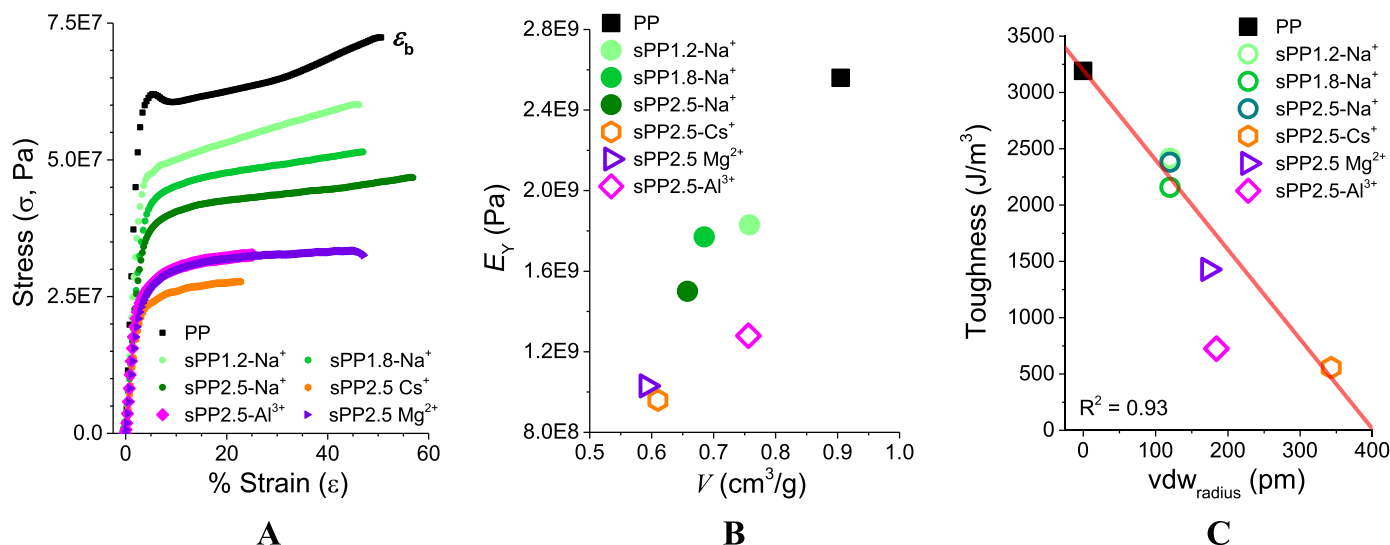


Fig. 6. PP and sPPx-M film A) tensile σ versus ϵ , B) E_Y versus V (cm^3/g), and C) Modulus of Toughness (Toughness) versus counter-ion $\text{vdw}_{\text{radius}}$.

Table 5

sPP2.5-M and experimentally observed $\nu(\text{SO}_3)$, $\nu(\text{SO}_2)$, and $\nu(\text{S-O})$; and predicted $\Delta E(\text{SO}_3)$, $\Delta E(\text{SO}_2)$, and $\Delta E(\text{S-O})$ versus sPP-2.5-H⁺.

	$\nu(\text{SO}_3)$ (cm ⁻¹)	$\nu_s(\text{SO}_2)$ (cm ⁻¹)	$\nu_s(\text{SO})$ (cm ⁻¹)	$\Delta E(\text{SO}_3)$ (J/mol)	$\Delta E(\text{SO}_2)$ (J/mol)	$\Delta E(\text{SO})$ (J/mol)
sPP2.5-H ⁺	1169	1125	1033	0.0	0.0	0.0
sPP2.5-Na ⁺	1175	1126	1036	71.8	12.0	35.9
sPP2.5-Cs ⁺	1176	1125	1034	83.7	12.0	12.0
sPP2.5-Mg ²⁺	1170	1127	1035	12.0	23.9	23.9
sPP2.5-Al ³⁺	1163	1126	1034	-71.8	12.0	12.0

Table 6

Nominal tensile stress-strain curves for sPP materials.

	WC ^c (wt%)	E_Y (GPa)	σ_{yield} (MPa)	ϵ_b (%)	Toughness (J/m ³)
PP	0.00	2.56	54.5	50.9	3190
sPP1.2-Na ⁺	9.50	1.83	47.3	46.5	2415
sPP1.8-Na ⁺	11.8	1.77	44.8	47.1	2157
sPP2.5-Na ⁺	16.3	1.50	40.7	57.2	2380
sPP2.5-Cs ⁺	12.0	0.96	23.9	23.1	555
sPP2.5-Mg ²⁺	24.9	1.03	29.6	47.4	1429
sPP2.5-Al ³⁺	16.7	1.28	31.7	25.7	724

* WC was determined by total weight loss after equilibrating at 200 °C.

overall these properties are lower than sPP2.5-Na⁺. While ionic crosslinks have the potential to improve material toughness and strength, previous studies have shown neutralization with alkaline and alkaline earth metals tends to lower properties that is consistent with this work [36,38]. For example, sPP2.5-Al³⁺ and sPP2.5-Mg²⁺ potential crosslinking with a multi-valent ion should have improved strength and resistance to failure. However, its high WC appears to contribute to its failure. Overall, E_Y and ϵ_b for sPP2.5-M increased with counter-ion in the following order: Na⁺ > Al³⁺ > Mg²⁺ > Cs⁺ (Figs. 6A and 6B).

Ionic interactions and ion-size impact upon ionomer film toughness were shown using sulfonated polystyrene complexed with metal ions [38,39]. This work revealed that increasing ion-size leads to a decreased film toughness that is consistent with our work. sPPx-M film modulus of toughness (Toughness) was determined by integrating their σ - ϵ curves that are summarized in Fig. 6C versus metal-ion's vdw_{radius} . sPPx-Na⁺ metal-ion complexed films led to materials with relatively the same Toughness that ranged from 2415 J/m³ (sPP1.2-Na⁺) to 2380 J/m³ (sPP2.5-Na⁺), which is a variation of less than 2%. The large Cs⁺ ion significantly reduced sPP2.5 film Toughness to 555 J/m³ for sPP2.5-Cs⁺. This is a 77% reduction in film strength that is due to

weakened ion domain strength caused by its size (vdw_{radius} 343 pm) and mass (312.91 g/mol). These factors contribute to an increase in the inter-ion distance between -SO₃Cs groups that suppressed ionic interactions contributing to film strength as noted by Navratil and Lefelar et al. [38,40] A linear fit was used to relate film Toughness as a function of the metal-ion's vdw_{radius} shown in Fig. 6C. A good fit is achieved with monovalent ion's, but it is apparent that sPP2.5-Al³⁺ does not have behavior similar to these ions. This is attributed its multi-valent characteristics previously discussed in terms of charge availability, its neutralization, and steric hindrances. All these factors impact potential crosslinking, and ultimately its strength. The sPP2.5-Mg²⁺ had film Toughness of 1429 J/m³ that would have been greater if not severely plasticized by H₂O (24.9 wt%). Its film Toughness was statistically close to this predicted line, but it is believed that removal of residual water at the same level as other sPP2.5-M samples would have led to a larger value. sPP2.5-M film Toughness trend as a function of counter-ion type was Na⁺ > Mg²⁺ > Al³⁺ > Cs⁺. These results reveal that solid-state exchanging different metal ion types and size into an ionomer has a large impact upon film strength.

PP and sPPx-M thermal relaxation behavior was investigated using DMA after equilibrating at 125 °C for 30 min to remove residual water (Fig. 7A). PP's film elastic storage modulus (E') changes with temperature showed a singular relaxation mode with an E of 1.91×10^9 Pa at 150 °C. A plot of its loss modulus (E'') versus temperature reveals a thermal alpha (α) relaxation temperature (T_α) at 392 °C (Fig. 7C). In contrast to PP, the sPPx-M film's E' increased with IEC due to ionic crosslinking. These interactions impede chain motion leading to improved resistance to deformation [29]. These enhanced interactions led to an increase in sPPx-M film's E' based upon counter-ion and sulfonation level at 150 °C in the following manner: sPP2.5-Mg²⁺ ($E' = 3.98 \times 10^9$ Pa) > sPP2.5-Al³⁺ (E' of 3.80×10^9 Pa) > sPP2.5-Na⁺ ($E' = 3.32 \times 10^9$ Pa) > sPP1.8-Na⁺ ($E' = 2.90 \times 10^9$ Pa) > sPP1.2-Na⁺ ($E' = 2.77 \times 10^9$ Pa). Increasing sPPx sulfonation level to create sPP1.2-Na⁺, sPP1.8-Na⁺, and sPP2.5-Na⁺ revealed a steady rise in E' , which indicates a stiffening of these ionomers. What is profound about this result is their failure to have a thermal relaxation as they approached their glass transition temperature (T_g). A material's T_g corresponds to the onset of long-range mobility as chains and functional groups overcome entanglements, and ionic interactions. However, this is not observed with any sPPx-M film, which suggests that these thermally induced motions require greater thermal energy. As previously discussed, sPP2.5-Cs⁺ film was a brittle material shown from σ - ϵ tests (Fig. 6A). This translated into failed DMA tensile-mode tests using it. Interestingly, this brittle material had the largest metal-ion/sulfonate vibrational energy change due to -SO₃Cs interactions leading to $\Delta E(\text{SO}_3) = 83.7$ J/mol (Table 5). sPP2.5-Mg²⁺ and sPP-2.5-Al³⁺ behavior were similar until the sPP2.5-Mg²⁺ film broke at 290 °C. Beyond this

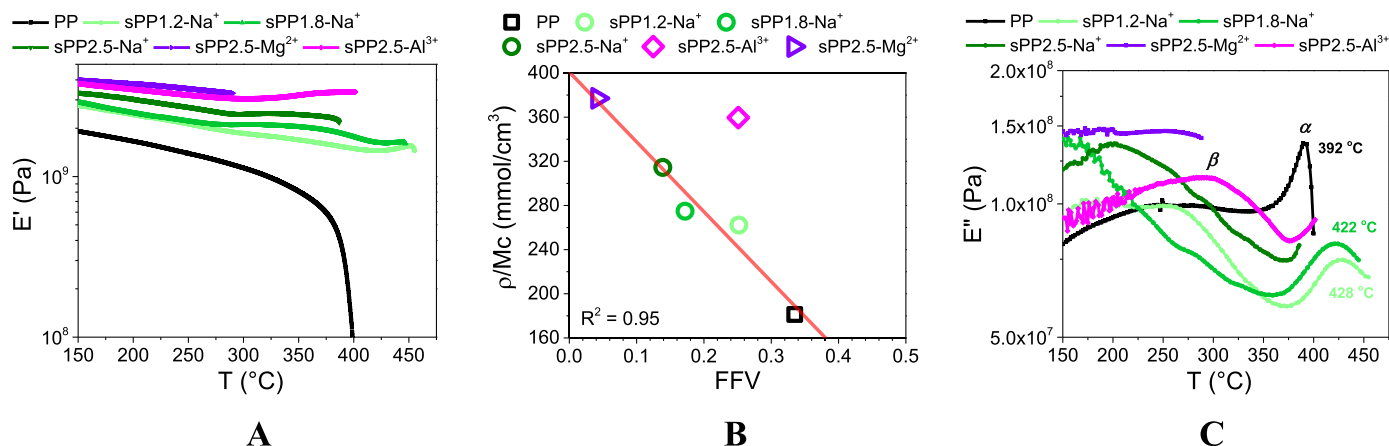


Fig. 7. DMA of sPPx-M films A) E' versus T , B) active chains per unit volume (ρ/Mc) versus FFV, and C) E'' versus T .

temperature, E' slowly rose for sPP2.5-Mg²⁺ with temperature until its failure at 400 °C that is close to the T_g of PP. This rise in E' with temperature is indicative of crosslinking that requires additional studies. The temperature that sPP1.2-Na⁺, sPP1.8-Na⁺, and sPP2.5-Na⁺ films broke at were 456 °C (sPP1.2-Na⁺), 448 °C (sPP1.8-Na⁺), and 388 °C (sPP2.5-Na⁺).

The observed E' plateau that extends beyond 298 °C is related to its entangled molecular weight network (M_c) and ρ . The molar concentration density of entangled network chains is ρ/M_c that is related to its modulus by $E' = 3RT\rho/M_c$. The predicted ρ/M_c evaluated using E' at 150 °C is shown in Fig. 7B versus FFV at 25 °C. The apparent ρ/M_c chain density increased with sulfonation and counter-ion concentration. Ionic crosslinking was observed with sPP2.5-Mg²⁺ noted by E'' that did not have a beta relaxation (β) temperature as observed with all sPPx-M films (Fig. 7C), which has been shown by Fan and Cornelius using divalent ions to crosslink PBC [11]. The highest ρ/M_c was 377 mmol/cm³ using sPP2.5-Mg²⁺ that decreased linearly with FFV (0.042) to 181 mmol/cm³ for PP (FFV = 0.335). FFV decreasing with increasing ρ/M_c is attributed to greater chain packing within a given unit volume that did not appear to influence the chain's predicted V_o summarized in Table 2. This seems to suggest the FFV associated with sPPx-M is very important to its physical properties as observed with epoxy based composites [41]. sPP-2.5-Al³⁺ did not follow PP, or mono and divalent complexed sPPx-M film's mechanical property changes with temperature. This is consistent with its deviation from all properties that has been attributed to all Al³⁺ charges being unable to crosslink with a sulfonate group.

A large β relaxation temperature is noted with sPP2.5-Al³⁺ ($T_\beta = 300$ °C), sPP2.5-Na⁺ ($T_\beta = 200$ °C), sPP1.8-Na⁺ ($T_\beta = 160$ °C), sPP1.2-Na⁺ ($T_\beta = 260$ °C), and PP ($T_\beta = 250$ °C) shown in Fig. 7C. This relaxation is typically associated with smaller side groups such as phenyl and sulfonated groups undergoing various degrees of “local” motion. The β relaxation temperature range appears to be unrelated to IEC, and may be due to processing effects noted by Wang and Cornelius using PBC [42]. However, this requires additional processing studies to validate this statement. The T_α relaxation temperature for sPP1.8-Na⁺, sPP1.2-Na⁺, and PP was 422 °C, 428 °C, and 392 °C. This thermal relaxation was not measureable due to film failure for sPP2.5-Al³⁺ and sPP2.5-Na⁺. Overall, functional group concentration density changes due to IEC and metal-ion led to varying degrees of restricted chain mobility and decreased FFV. The improved thermal resistance to material changes is an attractive trait for high temperature gas separations.

3.4. PP and sPPx-M gas transport properties

PP and sPPx-M films were used as gas separation membranes that had their permeability plotted versus kinetic diameter (KD) (Fig. 8A). KD has traditionally been used to characterize Knudsen Diffusion within mesoporous materials, and it may not be truly representative of a complex ionomer system [43]. However, it does provide a general guide to compare materials that has been done by numerous researchers [1–7,11–17,29–31]. PP and sPPx-Na⁺ film P behavior was compared to the KD of He (0.260 nm), H₂ (0.289 nm), CO₂ (0.33 nm), O₂ (0.346 nm), N₂ (0.364 nm), and CH₄ (0.380 nm) shown in Fig. 8A and summarized in Table 7. The gas permeability through these thin films had the following transport trend: $P_{CO_2} > P_{H_2} > P_{He} > P_{O_2} > P_{CH_4} > P_{N_2}$. PP had a P_{CO_2} (152 Barrer) and P_{H_2} (134 Barrer) that were larger than P_{He} (78.3), which does not scale with gas KD . sPP1.2-Na⁺ ($P_{CO_2} = 67.1$ Barrer and $P_{H_2} = 79.2$ Barrer) and sPP1.8-Na⁺ ($P_{CO_2} = 36.5$ Barrer and $P_{H_2} = 51.5$ Barrer) also had permeability that were not consistent with the gas diameter. This result suggests larger polymer-gas interactions impact D and S [11]. Increasing sulfonate group concentration (IEC) within sPPx-Na⁺ produced a material capable of greater hydrogen bonding noted as an increase in -SO₃H absorption intensity at 1169 cm⁻¹. This functional group led to decreasing ionomer gas permeability (sPP1.2-Na⁺ > sPP1.8-Na⁺ > sPP2.5-Na⁺) that affected the overall permeability trend in the following manner: $P_{H_2} > P_{He} > P_{O_2} > P_{N_2} > P_{CH_4}$. However, P_{CO_2} continually declined with IEC until it became less permeable than P_{H_2} for all sPPx-Na⁺. This trend clearly demonstrates the role of -SO₃H within a material upon gas transport. Similar efforts were shown by Cornelius *et al.* using a series of 6FDA-DABA polyimides with a -COOH group that modulated hydrogen bonding in order to improve gas permselectivity [44,45]. While all films tested had not residual water present within one to cause plasticization, it is speculated that a sPPx-M film plasticized with water may lead to greater gas permeability. However, such a material would have transient properties if its absorbed water concentration varied with temperature, pressure, relative humidity, and gas. These studies are beyond this work, but should be considered if scaling to complex industrial gas streams.

sPP1.2-Na⁺, sPP1.8-Na⁺, and sPP2.5-Na⁺ gas permeability versus sulfonate group concentration (IEC* ρ), and PP are shown in Fig. 8B. Sulfonating PP in order to create sPP1.2-H⁺, sPP1.8-H⁺, and sPP2.5-H⁺ caused its density to increase from 1.105 g/cm³ up to 1.413 g/cm³. This rise in ρ is directly proportional to IEC. In general, an increase in material density signifies tighter packing amongst polymer chains that

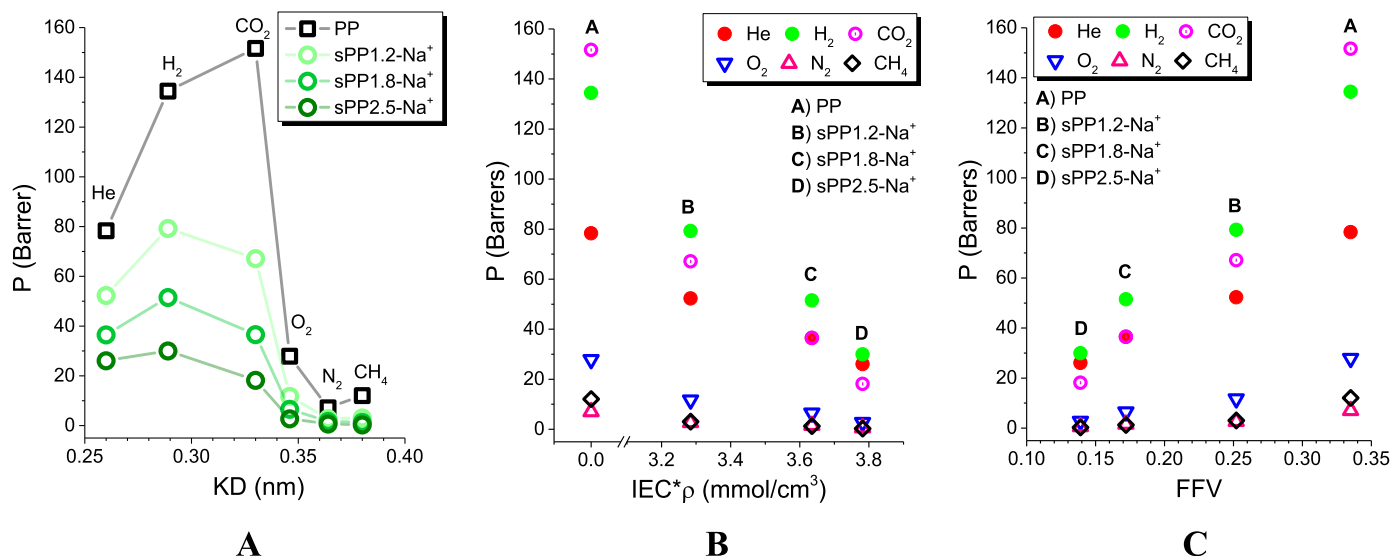


Fig. 8. PP and sPPx-Na⁺ film gas P versus A) KD , B) $IEC \cdot \rho$ and, C) FFV.

Table 7
Gas permeability and ideal selectivity of PP and sPPx-M.

	P (Barrer)					
	He	H ₂	CO ₂	O ₂	N ₂	CH ₄
PP	78.3	134	152	27.8	7.08	12.1
sPP1.2-Na ⁺	52.3	79.2	67.1	11.7	2.73	3.07
sPP1.8-Na ⁺	36.4	51.5	36.5	6.47	1.60	1.28
sPP2.5-Na ⁺	26.0	30.0	18.2	2.70	0.59	0.25
sPP2.5-Cs ⁺	17.7	21.3	11.6	1.80	0.21	0.23
sPP2.5-Mg ²⁺	13.6	16.8	6.95	0.92	0.11	0.08
sPP2.5-Al ³⁺	36.8	51.1	35.3	5.37	0.84	0.87

Evaluated at 30 °C and 4 atm (absolute). Overall error ~5% for permeability. $P = 10^{-10}(\text{cm}^3(\text{STP})\text{cm}/(\text{cm}^2 \text{ s cmHg}))$.

would negatively affect its total FFV. A linear trend of decreasing P with increasing $-\text{SO}_3\text{Na}$ group concentration is notable. This reduction reveals how hydrogen bonding reduces chain motion needed to accommodate molecule diffusion through an ionomer [7,11,13,17,20,46]. The general permeability trend is: sPP1.2-Na⁺ (1.61 mmol/cm³) > sPP1.8-Na⁺ (2.57 mmol/cm³) > sPP2.5-Na⁺ (3.75 mmol/cm³). This directly corresponds with $\text{IEC}^*\rho$ (mmol $-\text{SO}_3\text{H}/\text{cm}^3$ ionomer). PP ranged between 152 (P_{CO_2}) to 7.08 (P_{N_2}) Barrers that decreased 56% (sPP1.2-Na⁺) to 88% (sPP2.5-Na⁺) for P_{CO_2} , and 61% (sPP1.2-Na⁺) to 92% (sPP2.5-Na⁺) for P_{N_2} due to its sulfonation to create sPP2.5-H⁺. sPPx-Na⁺ and PP predicted FFV versus gas permeability is shown in Fig. 8C. sPP2.5-Na⁺ had the lowest FFV (0.139) that was coupled to the highest density and SO_3H absorption intensity, which was the least permeable material. In contrast to sPPx-H⁺, PP had the largest FFV (0.335), and the largest gas permeability. In general, increasing sulfonate group concentration within sPPx led to a decrease in FFV, and larger ρ that is related to chain packing density (Table 2).

Gas permeability through sPP2.5-M⁺ membrane versus KD had the following trend: $P_{\text{H}_2} > P_{\text{He}} > P_{\text{CO}_2} > P_{\text{O}_2} > P_{\text{N}_2} > P_{\text{CH}_4}$ (Fig. 9A). In general, P decreased with increasing KD with P_{H_2} being an exception to this observation. sPP2.5-M⁺ membrane permeability varied with cation size in the following manner: $\text{Na}^+ > \text{Cs}^+ > \text{Mg}^{2+}$. The sPP2.5-Mg²⁺ had the lowest gas permeability of the series ranging between $P_{\text{H}_2} = 16.8$ Barrer to $P_{\text{CH}_4} = 0.08$ Barrer. This behavior is similar to observations using N117-Ca²⁺ and PBC-Ca²⁺ by Fan and Cornelius [7,11] where divalent metal ion behavior deviated from monovalent correlations. These properties were attributed to changes in D and S due to ionic cross-links

not possible with a monovalent ion. sPP2.5-Na⁺ membrane permeability was 157–14.7% greater than sPP2.5-Cs⁺ for N₂ and He ($P_{\text{N}_2} = 0.54$ and 0.21 Barrer; and $P_{\text{He}} = 20.3$ and 17.7 Barrer). Overall, these results suggest that permeability differences may be due to counter-ion size. However, sPP2.5-Al³⁺ had permeability that was not expected due to valence and size ranging from 51.1 to 36.8 Barrers using H₂ and He. The sPP2.5-Al³⁺ membrane deviation is attributed to changes in $\text{IEC}^*\rho$ and FFV. The role of changing sulfonate group density and its impact to material FFV is shown in Fig. 9B and Fig. 9C. These results clearly reveal that increasing $\text{IEC}^*\rho$ produces an equivalent loss in FFV that is needed for gas transport. The permeability trend was sPP2.5-Al³⁺ > sPP2.5-Na⁺ > sPP2.5-Cs⁺ > sPP2.5-Mg²⁺ with $P_{\text{H}_2} > P_{\text{He}} > P_{\text{CO}_2} > P_{\text{O}_2} > P_{\text{N}_2} > P_{\text{CH}_4}$. Counter-ion type appears to be an important factor that governs the permeability behavior of an ionomer. sPPx-M permeability behavior is clearly a function of IEC and counter-ion that affects FFV. The sulfonated domains are less permeable, which appears to enhance “molecular sieving” due to decreased diffusive pathways, and suppressed gas solubility in the material. Overall, a direct correlation between gas permeability and counter-ion size was not clearly apparent with these materials.

The ideal gas S_{CO_2} , S_{CH_4} , D_{CO_2} , and D_{CH_4} , for sPPx-M was estimated using the time-lag method and compared to its FFV shown Fig. 10 [31]. In general, S_{CH_4} increased with IEC, but S_{CO_2} appeared to be unaffected by counter-ion type and IEC. One approach to explain gas solubility behavior is its correlation to condensability represented by its critical temperature, which is 304 K and 190 K for CO₂ and CH₄. Another explanation is molecular interactions between chains, and domains that impacts gas solubility. This is attributed to changes in its enthalpy of mixing and FFV altering entropy [47]. Consequently; these solubility trends are attributed to sulfonic group dynamics that are modulated by its counter-ion altering gas absorption due to entropic effects and FFV. Interestingly, increasing gas solubility with metal cation has the following behavior for sPP2.5-M: $\text{Na}^+ < \text{Cs}^+ < \text{Al}^{3+} < \text{Mg}^{2+}$. This behavior is a dynamic and complex process involving chain mobility, metal-ion and sulfonate group complexation strength, losses in FFV, and sulfonate group concentration. Additional studies beyond this work are needed to explore this phenomenon. The parent PP exhibits moderate solubility and high diffusivity that are comparable to other phenylated amorphous/glassy polymers such as poly(phenylene oxide) and its derivatives [12–14,25]. A decrease in gas D with sPPx-M IEC reveals that the ionic domains are impeding gas transport due to reduced chain mobility. Consequently, increasing IEC within sPP produces a less permeable material caused by a reduction in gas diffusion that is noted with these ionomers [11–17,25,29–31,42,46]. Monovalent metal-ion

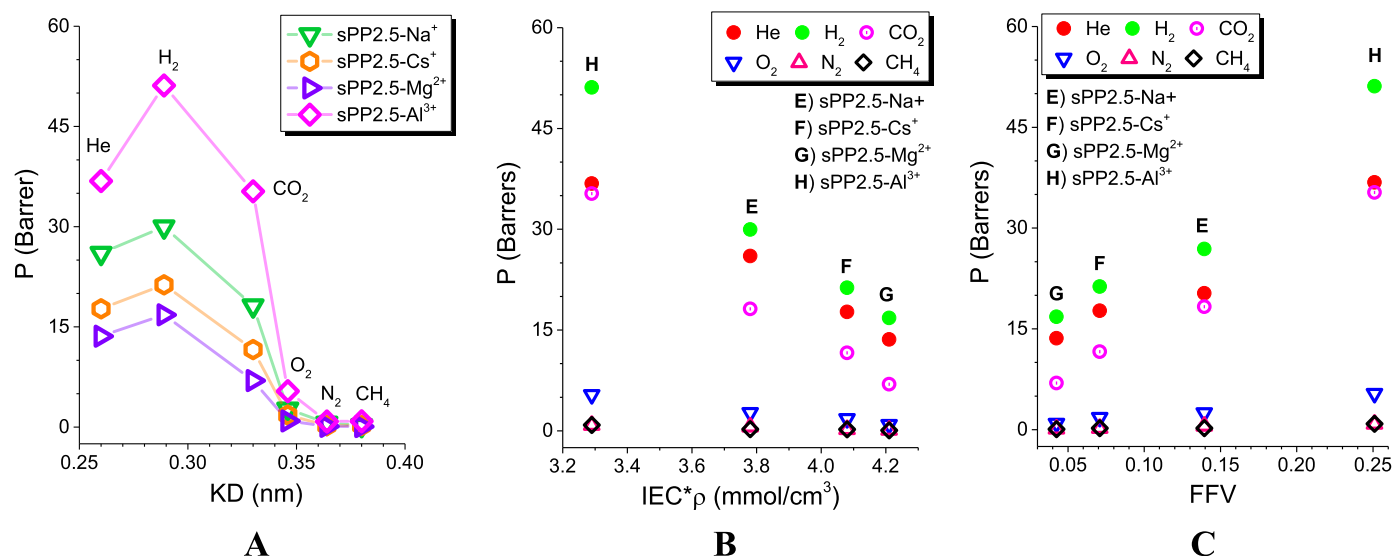


Fig. 9. sPP2.5-M film gas P versus A) KD , B) $\text{IEC}^*\rho$, and C) FFV.

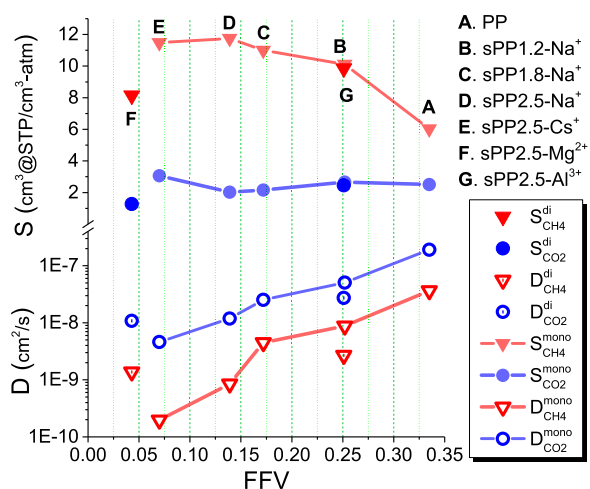


Fig. 10. PP and sPPx-M gas D and S for CO_2 and CH_4 .

substitution into sPPx-M led to a significant decrease in gas diffusivity. Utilization of multi-valent ions Mg^{2+} and Al^{3+} caused a reduction in sPP2.5-M, but not at the same level as sPP2.5- Cs^+ . Gas diffusivity through sPP2.5-M had the following trend for CH_4 and CO_2 : $\text{Na}^+ > \text{Al}^{3+} > \text{Mg}^{2+} > \text{Cs}^+$. The treated materials display a decrease in diffusivity with increasing counter ion size ($\text{Mg}^{2+} > \text{Na}^+ > \text{Cs}^+$) indicating that the larger ions occupy greater free volume blocking the diffusing species. A general trend for S and D appears to be present with the monovalent ions, but not of Mg^{2+} and Al^{3+} .

sPPx-M and PP film gas permselectivity trade-offs for CO_2/CH_4 and O_2/N_2 were compared to Robeson's 1991 and 2008 upper bounds [48] shown in Fig. 11. sPPx-M film's CO_2/CH_4 gas selectivity (α) consistently increases as a function of IEC that is significantly greater than PP ($\alpha = 12.6$) shown in Fig. 11A. sPP2.5- Cs^+ and sPP2.5- Al^{3+} improved permeability, but it came at a loss in CO_2/CH_4 selectivity ($\alpha = 50.4$ and 40.6) relative to sPP2.5- Na^+ ($\alpha = 83.2$). The largest improvement was noted with sPP2.5- Mg^{2+} ($\alpha = 86.9$) with decreased permeability. The improvement in gas selectivity is ascribed to ionic crosslinking observed during DMA tests (Fig. 7C). The O_2/N_2 gas selectivity behavior using sPPx- Na^+ films were weakly dependent upon IEC, but O_2 gas permeability decreased with IEC (Fig. 11B). sPP2.5- Cs^+ and sPP2.5- Mg^{2+} had a very large O_2/N_2 selectivity of 8.57 and 8.36, which is nearly twice as large as sPP2.5- Na^+ and PP ($\alpha = 4.58$ and 3.93). The sPP2.5- Al^{3+}

membrane had a simultaneous improvement in O_2 permeability ($P = 5.37$ Barrer) and O_2/N_2 selectivity ($\alpha = 6.37$) relative to sPP2.5- Na^+ ($P = 2.7$ Barrer). Overall, these metal-ion neutralized sPP2.5-M membrane's permselectivity performances were not directly related to counter-ion size. For example, sPP2.5- Na^+ is the best membrane for a CO_2/CH_4 , but sPP2.5- Mg^{2+} has the greatest O_2/N_2 performance. It is noteworthy that a material with a wide range of gas pair permselectivity indicates substantial separation tune-ability. Sulfonated PP has comparable performance to a 6FDA-6FpDA polyimide membrane that has received considerable attention due to high gas permselectivity [29,30,44,45,49,50]. While sulfonation was proven to be an incredibly effective approach to alter gas transport properties, there exists numerous facile chemical and physical modifications such as bromination [13,51], polymer blending [52], nitration and amination [25], and nanocomposites composites that have technical merit for industrial gas separations [39].

4. Conclusions

A sPP ionomer series physical, thermal, and ideal gas transport properties were studied as a function of ion concentration, and metal counter-ion size and type. The parent PP material had a T_g at 391°C that increased to approximately 420°C upon sulfonation and complexation with a metal-ion. An FT-IR analysis revealed a correlation between asymmetric sulfonic adsorption $\Delta\nu(\text{SO}_3^-)$ and ion size due to metal counter-ion. Sulfonated film thermal stability exhibited a sharp degradation step above 560°C that decreased with ion content. Thermal and mechanical stability increased with the metal-ion type in the following order: $\text{Na}^+ > \text{Al}^{3+} > \text{Mg}^{2+} > \text{Cs}^+$. PP exhibited high gas permeability and moderate selectivity. Increasing IEC produced films with decreased gas diffusivity. sPPx-M membrane O_2 solubility increased, but CO_2 decreased within it. This result may suggest entropic limitations are associated with larger gas molecules due to decreased FFV. In general, gas solubility increased with counter-ion size indicating a potential correlation with metal-ion complex strength. The observed phenomena resulted in a wide variation in gas selectivity whereby optimal performance was largely a function of the gas pair. These materials have sufficient thermal and mechanical properties for more aggressive gas separations that are tune-able using metal counter-ions. Consequently, sPP materials are potentially competitive candidates for some industrial gas separations.

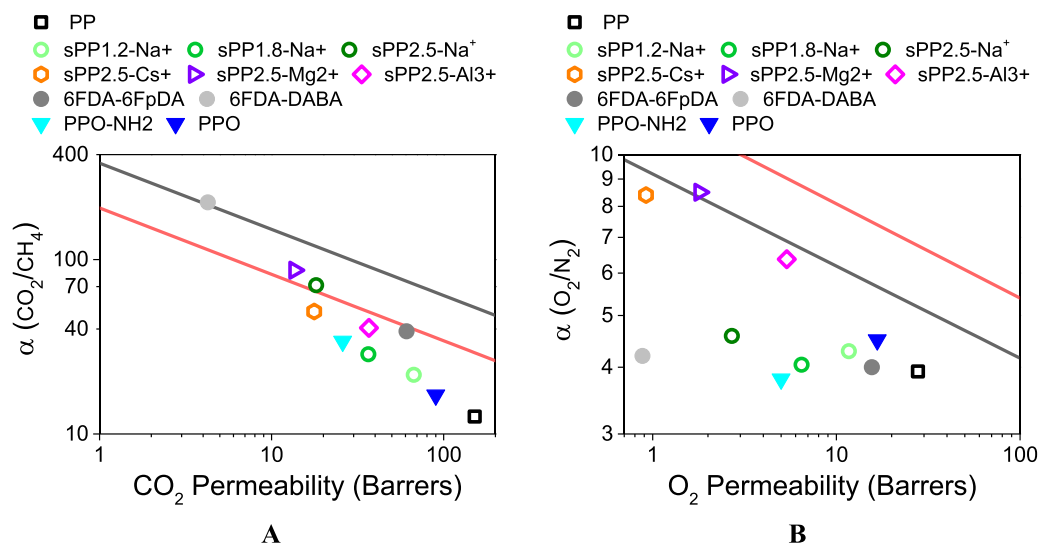


Fig. 11. A) Ideal CO_2/CH_4 gas selectivity versus CO_2 permeability, and B) O_2/N_2 ideal selectivity versus O_2 permeability trade-off performance for sPPx-M compared to PPO, PPO-NH₂, 6FpDA-6FDA, and 6FDA-DABA [12,25,44,53].

Acknowledgments

The author would like UNL and US Department of Education: Graduate Assistance in Areas of National Need for financial support of this work. A portion of this work was possible due to funding by a grant from the Nebraska Center for Energy Sciences Research at the University of Nebraska-Lincoln.

References

- [1] F.G. Kerry Industrial Gas Handbook: Gas Separation and Purification, Taylor and Francis Group, LLC.
- [2] Y. Jeon, D. Lee, Gas membranes for CO₂/CH₄ (biogas) separation: a review, *Environ. Eng. Sci.* 32 (2015) 1–15.
- [3] S. Sridhar, B. Smitha, T.M. Aminabhavi, Separation of carbon dioxide from natural gas mixtures through polymeric membranes—a review, *Sep. Purif. Rev.* 36 (2007) 113–174.
- [4] P. Bernardo, E. Drioli, G. Golemme, Membrane gas separation: a review/state of the art, *Ind. Eng. Chem. Res.* 48 (2009) 4638–4663.
- [5] Y. Zhang, J. Sunarso, S. Liu, R. Wang, Current status and development of membranes for CO₂/CH₄ separation: a review, *Int. J. Greenh. Gas Control.* 12 (2013) 84–107.
- [6] D. Aaron, C. Tsouris, From flue gas: a review, *Sep. Sci. Technol.* 40 (2005) 321–348.
- [7] Y. Fan, D. Tongren, C.J. Cornelius, The role of a metal ion within Nafion upon its physical and gas transport properties, *Eur. Polym. J.* 50 (2014) 271–278.
- [8] L.G. Lage, P.G. Delgado, Y. Kawano, Thermal stability and decomposition of nafion membranes with different cations using high-resolution thermogravimetry, *J. Therm. Anal. Calorim.* 75 (2004) 521–530.
- [9] D.L. Feldheim, D.R. Lawson, C.R. Martin, Influence of the sulfonate counterion on the thermal stability of nafion perfluorosulfonate membranes, *J. Polym. Sci. Part B Polym. Phys.* 31 (1993) 953–957.
- [10] T. Sakai, H. Takenaka, E. Torikai, Gas diffusion in the dried and hydrated nafions, *J. Electrochem. Soc.* 133 (1986) 88–92.
- [11] Y. Fan, C.J. Cornelius, Raman spectroscopic and gas transport study of a pentablock ionomer complexed with metal ions and its relationship to physical properties, *J. Mater. Sci.* 48 (2013) 1153–1161.
- [12] B. Kruzeczek, T. Matsuura, Effect of metal substitution of high molecular weight sulfonated polyphenylene oxide membranes on their gas separation performance, *J. Membr. Sci.* 167 (2000) 203–216.
- [13] F. Hamad, T. Matsuura, Performance of gas separation membranes made from sulfonated brominated high molecular weight poly(2,4-dimethyl-1,6-phenylene oxide), *J. Membr. Sci.* 253 (2005) 183–189.
- [14] J.-W. Rhim, G. Chowdhury, T. Matsuura, Development of thin-film composite membranes for carbon dioxide and methane separation using sulfonated poly(phenylene oxide), *J. Appl. Polym. Sci.* 76 (5) (2000) 735–742.
- [15] W. Chen, C. Martin, Gas-transport properties of sulfonated polystyrenes, *J. Membr. Sci.* 95 (1994) 51–61.
- [16] H.B. Park, S.Y. Nam, J.W. Rhim, J.M. Lee, S.E. Kim, J.R. Kim, Y.M. Lee, Gas-transport properties through cation-exchanged sulfonated polysulfone membranes, *J. Appl. Polym. Sci.* 86 (2002) 2611–2617.
- [17] Y. Fan, M. Zhang, R.B. Moore, C.J. Cornelius, Structure, physical properties, and molecule transport of gas, liquid, and ions within a pentablock copolymer, *J. Membr. Sci.* 464 (2014) 179–187.
- [18] T.D. Largier, C.J. Cornelius, Random quaternary ammonium diels-alder poly(phenylene) copolymers for improved vanadium redox flow batteries, *J. Power Sources* 352 (2017) 149–155.
- [19] T.D. Largier, D. Wang, J. Mueller, C.J. Cornelius, Improving electrodialysis based water desalination using a sulfonated Diels-Alder poly(phenylene), *J. Membr. Sci.* 531 (2017) 103–110.
- [20] T. Largier, F. Huang, C.J. Cornelius, Homopolymer and multi-block diels-alder polyphenylenes: synthesis, physical properties, X-ray diffraction, and gas transport, *Eur. Polym. J.* 89 (2017) 301–310.
- [21] H. Lilin, C.J. Cornelius, D. Perahia, Water dynamics in highly rigid ionomers, *Eur. Polym. J.* 56 (2014) 168–173.
- [22] R.J. Stanis, M.A. Yaklin, C.J. Cornelius, T. Takatera, A. Umamoto, A. Ambrosini, C.H. Fujimoto, Evaluation of hydrogen and methanol fuel cell performance of sulfonated diels alder poly(phenylene) membranes, *J. Power Sources* 195 (2010) 104–110.
- [23] H. Lilin, C.H. Fujimoto, C.J. Cornelius, D. Perahia, From solutions to membranes: structure studies of sulfonated polyphenylene ionomers, *Macromolecules* 42 (2009) 7084–7090.
- [24] M. Hibbs, C.H. Fujimoto, C.J. Cornelius, Synthesis and characterization of poly(phenylene)-based anion exchange membranes for alkaline fuel cells, *Macromolecules* 42 (2009) 8316–8321.
- [25] Y.S. Bhole, P.B. Karadkar, U.K. Kharul, Nitration and amination of polyphenylene oxide: synthesis, gas sorption and permeation analysis, *Eur. Polym. J.* 43 (2007) 1450–1459.
- [26] C.H. Fujimoto, M.A. Hickner, C.J. Cornelius, D.A. Loy, Ionomeric poly(phenylene) prepared by diels-alder polymerization: synthesis and physical properties of a novel polyelectrolyte, *Macromolecules* 38 (2005) 5010–5016.
- [27] G.K. Noren, J.K. Stille, Polyphenylenes, *J. Polym. Sci. Macromol. Rev.* 5 (1971) 385–430.
- [28] J. Stille, R.O. Rakutis, H. Mukamal, F.W. Harris, Diels-alder polymerizations. IV. Polymers containing short phenylene blocks connected by alkylene units, *Macromolecules* 1 (1968) 431–436.
- [29] C.J. Cornelius, E. Marand, Hybrid silica-polyimide membranes: gas transport properties, *J. Membr. Sci.* 202 (1–2) (2002) 97–118.
- [30] C.J. Cornelius, Physical and Gas Permeation Properties of a Series of Novel Hybrid Inorganic-Organic Composites based on a Synthesized Fluorinated Polyimide, PhD Dissertation, Virginia Tech, 2000.
- [31] J. Alexopoulos, J. Barrie, D. Machin, The time lag for the diffusion of gas mixtures, *Polymer* 10 (1969) 265–269.
- [32] N. Colthup, Introduction to Infrared and Raman Spectroscopy, Elsevier, 2012.
- [33] J.F. Blanco, Q.T. Nguyen, P. Schaezel, Novel hydrophilic membrane materials: sulfonated polyethersulfone Cardo, *J. Membr. Sci.* 186 (2) (2001) 267–279.
- [34] G. Socrates, Infrared and Raman Characteristic Group Frequencies: Tables and Charts, 3rd edition, John Wiley, 2001.
- [35] G.M. Geise, C.L. Willis, C.M. Doherty, A.J. Hill, T.J. Bastow, J. Ford, K.I. Winey, B.D. Freeman, D.R. Paul, Characterization of aluminum-neutralized sulfonated styrenic pentablock copolymer films, *Ind. Eng. Chem. Res.* 52 (2013) 1056–1068.
- [36] S.A. Visser, S.L. Cooper, Effect of neutralizing cation type on the morphology and properties of model polyurethane ionomers, *Polymer* 33 (1992) 920–929.
- [37] C. Bas, L. Reymond, A.-S. Danérol, N.D. Albérola, E. Rossinot, L. Flandin, Key counter ion parameters governing polluted nafion membrane properties, *J. Polym. Sci. Part B Polym. Phys.* 47 (2009) 1381–1392.
- [38] M. Navratil, A. Eisenberg, Ion clustering and viscoelastic relaxation in styrene-based ionomers. 111. Effect of counterions, carboxylic groups, and plasticizers, *Macromolecules* 7 (1) (1974) 84–89.
- [39] B.H. Calhoun, R.B. Moore, Dynamic mechanical properties of lightly sulfonated polystyrene ionomers, *J. Vinyl Addit. Technol.* 2 (4) (1996) 358–362.
- [40] J.A. Lefelar, R.A. Weiss, Concentration and counterion dependence of cluster formation in sulfonated polystyrene, *Macromolecules* 1148 (1984) 1145–1148.
- [41] G.M. Odegard, A. Bandyopadhyay, Physical aging of epoxy polymers and their composites, *J. Polym. Sci. Part B: Polym. Phys.* 49 (24) (2011) 1695–1716.
- [42] D. Wang, Y. Fang, M. Zhang, R.B. Moore, C.J. Cornelius, Ionomer solution to film solidification dependence upon solvent type and its impact upon morphology and ion transport, *Eur. Polym. J.* 97 (2017) 169–177.
- [43] S.A. Reinecke, B.E. Sleep, Knudsen diffusion, gas permeability, and water content in an unconsolidated porous medium, *Water Resour. Res.* 38 (12) (2002) 161–1615.
- [44] C.J. Cornelius, E. Marand, Hybrid inorganic-organic materials based on a 6FDA-6FpDA-DABA polyimide and silica: physical characterization studies, *Polymer* 43 (2002) 2385–2400.
- [45] F. Huang, A.T. Rad, M.-P. Neih, C.J. Cornelius, Hybrid organic-inorganic 6FDA-6FpDA and multi-block 6FDA-DABA polyimide SiO₂-TiO₂ nanocomposites: synthesis, FFV, FTIR, swelling, stability, and X-ray scattering, *Polymer* 108 (2017) 105–120.
- [46] Y. Fan, C.J. Cornelius, H.-S. Lee, J.E. McGrath, M. Zhang, R. Moore, C.L. Staiger, The effect of block length upon structure, physical properties, and transport within a series of sulfonated poly(arylene ether sulfone)s, *J. Membr. Sci.* 430 (2013) 106–112.
- [47] N.F.A. Van der Vegt, V.A. Kusuma, B.D. Freeman, Basis of solubility versus TC correlations in polymeric gas separation membranes, *Macromolecules* 43 (2010) 1473–1479.
- [48] L.M. Robeson, The upper bound revisited, *J. Membr. Sci.* 320 (2008) 390–400.
- [49] W. Qiu, L. Xu, C.-C. Chen, D.R. Paul, W.J. Koros, Gas separation performance of 6FDA-based polyimides with different chemical structures, *Polymer* 54 (2013) 6226–6235.
- [50] K.J. Kim, S.H. Park, W.W. So, D.J. Ahn, S.J. Moon, CO₂ separation performances of composite membranes of 6FDA-based polyimides with a polar group, *J. Membr. Sci.* 211 (2003) 41–49.
- [51] B. Yu, H. Cong, X. Zhao, Hybrid brominated sulfonated poly(2,6-diphenyl-1,4-phenylene oxide) and SiO₂ nanocomposite membranes for CO₂/N₂ separation, *Prog. Nat. Sci. Mater. Int.* 22 (2012) 661–667.
- [52] Y. Maeda, D.R. Paul, Selective gas transport in miscible PPO-PS blends, *Polymer* 26 (1985) 2055–2063.
- [53] F. Huang, C.J. Cornelius, Polyimide-SiO₂-TiO₂ nanocomposite structural study probing free volume, physical properties, and gas transport, *J. Membr. Sci.* 542 (2017) 110–122.